Supporting Information

A-π-A type quasi-macromolecular acceptors with molecular conjugation length control strategy for high-performance organic solar cells

Siqing He[1], Changhao Xiang[2], Wei Liu[1], Songting Liang[1], Rui Zhang[3], Weikun Chen[1], Bin Zhao[2], Jun Yuan[1] & Yingping Zou[1]*

[1]College of Chemistry and Chemical Engineering, Central South University, Changsha 410083, P. R. China

* E-mail: junyuan@csu.edu.cn

[2]College of Chemistry, Xiangtan University, Xiangtan 411105, P. R. China

[3]Department of Physics, Chemistry and Biology, Linköping University, Linköping SE-58183, Sweden

1. Experimental Section

Materials and Synthesis

All reagents and chemicals were purchased from Energy Chemical., and Titan, etc, and used as received without further purification unless otherwise specified. 5,5'-bis(trimethylstannyl)-2,2'-bithiophene and 5,5''-bis(trimethylstannyl)-2,2':5',2''-terthiophene were purchased from Derthon Optoeletronics Materials Science Technology Co LTD. 2-(5-bromo-3-oxo-2,3-dihydro-1H-inden-1-ylidene)malononitrile was purchased from Nanjing Zhiyan Technology Co.，Ltd. 2-(5,6-difluoro-3-oxo-2,3-dihydro-1H-inden-1-ylidene) malononitrile was purchased from HWRK Chem Co.，Ltd. Anhydrous toluene were distilled from Na with benzophenone as an indicator under argon. BTP-CHO, BTP-2F-Br, **QM-1T** were prepared according to the reported works before. The detailed synthetic procedures of these compounds and polymers are shown as followings.

Synthesis of QM-1T (QM1)

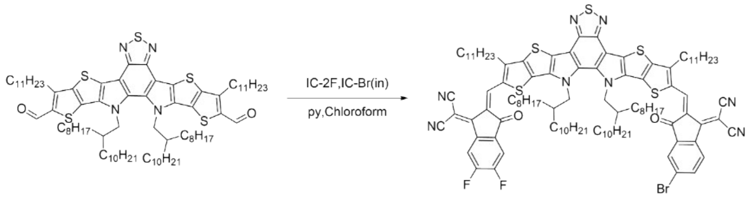

Figure S1. Synthetic route of BTP-2F-Br.

The synthetic procedure of BTP-2F-Br is detailed in our previous work[1].

^{1}H NMR (400 MHz, Chloroform-*d*) δ 9.18 (d, *J* = 7.8 Hz, 2H), 8.58 (dd, *J* = 9.1, 4.9 Hz, 2H), 8.04 (d, *J* = 1.9 Hz, 1H), 7.87 (dd, *J* = 8.4, 2.0 Hz, 1H), 7.70 (t, *J* = 7.5 Hz, 1H), 4.77 (d, *J* = 7.8 Hz, 4H), 3.23 (t, *J* = 8.1 Hz, 4H), 2.12 (p, *J* = 6.7 Hz, 2H), 1.88 (p, *J* = 7.7 Hz, 4H), 1.54 (d, *J* =

7.9 Hz, 4H), 1.27 (s, 30H), 1.15 (t, *J* = 7.4 Hz, 19H), 1.07 – 0.91 (m, 34H), 0.91 – 0.73 (m, 26H).

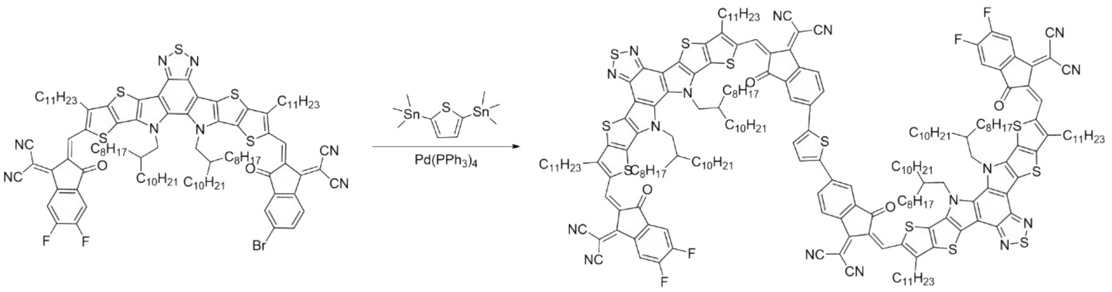

Figure S2. Synthetic route of **QM-1T** (**QM1**).

The synthetic procedure of **QM-1T** (**QM1**) is detailed in our previous work[1].

^{1}H NMR (400 MHz, Chloroform-*d*) δ 9.14 (d, *J* = 9.6 Hz, 4H), 8.75 (d, *J* = 8.2 Hz, 2H), 8.57 (dd, *J* = 9.9, 6.4 Hz, 2H), 8.11 (s, 2H), 7.97 (d, *J* = 8.4 Hz, 2H), 7.70 – 7.61 (m, 4H), 4.81 (d, *J* = 7.8 Hz, 8H), 3.21 (s, 8H), 2.17 (q, *J* = 6.2 Hz, 4H), 1.88 (h, *J* = 7.5 Hz, 8H), 1.50 (d, *J* = 7.7 Hz, 7H), 1.39 (d, *J* = 7.8 Hz, 8H), 1.27 (s, 49H), 1.24 – 1.09 (m, 53H), 1.02 (d, *J* = 8.5 Hz, 69H), 0.93 – 0.72 (m, 42H). ^{13}C NMR (101 MHz, $CDCl_3$) δ 187.76, 185.97, 159.56, 158.60, 153.84, 153.38, 147.45, 145.19, 145.17, 143.84, 138.94, 137.99, 137.79, 137.62, 136.14, 135.64, 135.04, 134.44, 134.27, 133.82, 133.54, 133.23, 131.19, 130.91, 130.46, 127.22, 126.04, 120.71, 119.72, 118.91, 115.42, 115.15, 114.96, 114.55, 113.80, 113.47, 68.60, 67.59, 55.77, 39.22, 31.94, 31.86, 31.25, 31.20, 30.62, 29.91, 29.83, 29.72, 29.69, 29.67, 29.65, 29.60, 29.56, 29.48, 29.42, 29.38, 29.29, 29.26, 25.70, 22.71, 22.66, 14.13. MALDI-TOF MS: calcd for $C_{216}H_{272}F_4N_{16}O_4S_{11}$ 3583.851, found 3583.720.

Synthesis of QM-2T

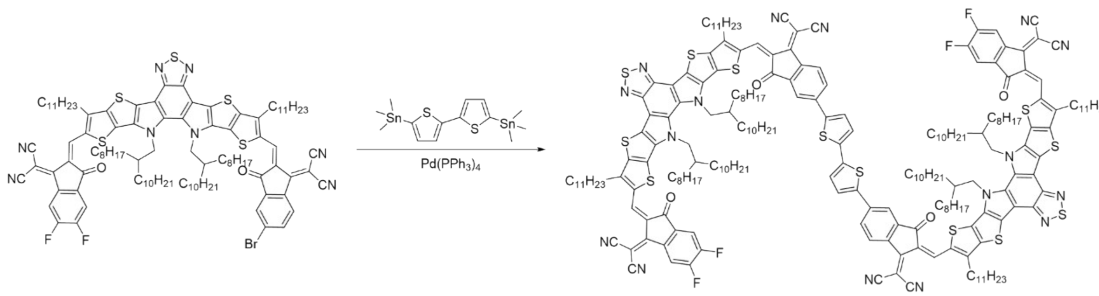

Figure S3. Synthetic route of **QM-2T**.

BTP-2F-Br (274 mg, 0.15 mmol), 5,5'-bis(trimethylstannyl)-2,2'-bithiophene (36.9 mg, 0.075 mmol) and $Pd(PPh_3)_4$ (4mg) were dissolved in 20 mL anhydrous and deoxidized toluene, then the mixture was stirred at 110 °C for 12 h under argon. After the reaction cooled to room temperature, solvent was removed by rotary evaporation. Then, the residue was extracted with dichloromethane and dried with anhydrous sodium sulfate, and then purified by column chromatography with petroleum ether/ dichloromethane (1:1, v/v) as an eluent. The blue black solid was obtained with a yield of 61 % (167 mg, 0.046 mmol). ^1H NMR (400 MHz, Chloroform-*d*) δ 9.13 (s, 2H), 9.10 (s, 2H), 8.70 (d, *J* = 8.2 Hz, 2H), 8.60 – 8.50 (m, 2H), 8.07 (s, 2H), 7.90 (d, *J* = 8.2 Hz, 2H), 7.60 (t, *J* = 7.5 Hz, 2H), 7.54 (d, *J* = 3.9 Hz, 2H), 7.35 (s, 2H), 4.79 (d, *J* = 15.1 Hz, 8H), 3.34 – 3.04 (m, 8H), 2.21 (s, 4H), 1.87 (s, 8H), 1.54 (s, 12H), 1.26 (d, *J* = 6.1 Hz, 64H), 1.15 (d, *J* = 27.8 Hz, 46H), 1.03 (s, 60H), 0.91 – 0.75 (m, 48H). ^{13}C NMR (101 MHz, $CDCl_3$) δ 187.87, 185.93, 159.67, 153.85, 153.16, 147.50, 147.44, 145.13, 145.11, 141.37, 139.14, 138.94, 138.50, 137.96, 137.77, 137.63, 136.12, 135.42, 134.27, 133.72, 133.46, 133.22, 130.92, 130.24, 125.77, 120.91, 119.69, 115.26, 113.74, 113.44, 77.33, 77.01, 76.70, 68.60, 67.37, 55.78, 39.14, 31.93, 31.90, 31.85, 31.27, 31.15, 30.56, 29.91, 29.88, 29.84, 29.71, 29.68, 29.66, 29.64, 29.61, 29.58, 29.55, 29.51, 29.48, 29.44, 29.37, 29.28, 29.26, 25.68, 22.70, 22.66, 14.13. MALDI-TOF MS: calcd for $C_{220}H_{274}F_4N_{16}O_4S_{12}$ (M^+), 3667.43; found, 3667.122.

Synthesis of QM-3T

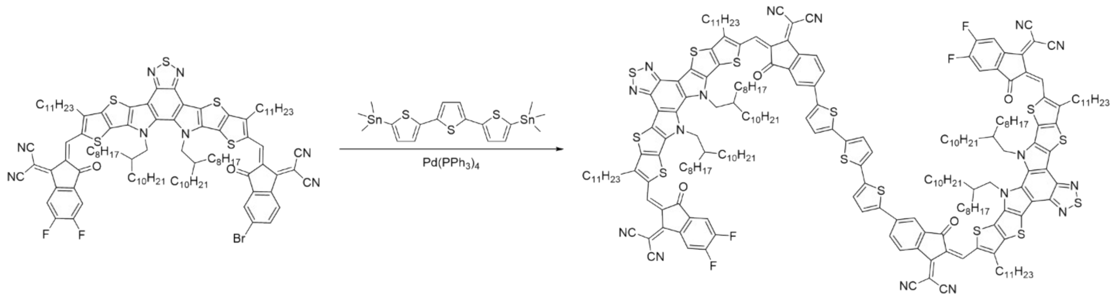

Figure S4. Synthetic route of **QM-3T**.

BTP-2F-Br (274 mg, 0.15 mmol), 5,5''-bis(trimethylstannyl)-2,2':5',2''-terthiophene (43 mg, 0.075 mmol) and $Pd(PPh_3)_4$ (4mg) were dissolved in 20 mL anhydrous and deoxidized toluene, then the mixture was stirred at 110 °C for 12 h under argon. After the reaction cooled to room temperature, solvent was removed by rotary evaporation. Then, the residue was extracted with dichloromethane and dried with anhydrous sodium sulfate, and then purified by column chromatography with petroleum ether/ dichloromethane (1:1, v/v) as an eluent. The blue black solid was obtained with a yield of 66 % (185 mg, 0.049 mmol). ^{1}H NMR (400 MHz, Chloroform-*d*) δ 9.07 (s, 2H), 8.99 (s, 2H), 8.62 (d, *J* = 7.9 Hz, 2H), 8.50 (d, *J* = 9.1 Hz, 2H), 7.86 (s, 2H), 7.80 (d, *J* = 7.7 Hz, 2H), 7.64 (t, *J* = 7.5 Hz, 2H), 7.48 (s, 2H), 7.22 (s, 2H), 7.14 (s, 2H), 4.89 (s, 8H), 3.27 (s, 8H), 2.31 (s, 4H), 1.83 (s, 8H), 1.54 (s, 12H), 1.31 (d, *J* = 39.7 Hz, 77H), 1.22 – 1.08 (m, 67H), 1.05 – 0.92 (m, 32H), 0.90 – 0.76 (m, 40H). ^{13}C NMR (101 MHz, $CDCl_3$) δ 186.47, 184.90, 157.59, 152.86, 152.00, 146.46, 144.16, 144.08, 139.72, 138.09, 137.31, 136.98, 136.51, 135.34, 135.15, 134.38, 133.30, 132.62, 132.43, 132.18, 130.00, 129.19, 125.69, 124.86, 124.23, 119.88, 118.59, 114.47, 114.21, 113.96, 113.58, 112.83, 112.39, 76.31, 75.99, 75.67, 67.50, 66.27, 54.79, 38.22, 30.91, 30.83, 30.21, 30.09, 29.67, 28.87, 28.70, 28.66, 28.62, 28.60, 28.57, 28.53, 28.48, 28.45, 28.42, 28.36, 28.28, 28.24, 24.79, 21.68, 21.63, 13.10. MALDI-TOF MS: calcd for $C_{224}H_{276}F_4N_{16}O_4S_{13}$ (M^+), 3749.55; found, 3749.390.

2. Instruments and Measurements

^1H NMR and ^{13}C NMR spectra were recorded using a Bruker AV-400 spectrometer in a deuterated chloroform solution at 298 K, unless specified otherwise. Chemical shifts are reported as δ values (ppm) with tetramethylsilane (TMS) as the internal reference. The molecular mass was confirmed using an Autoflex III matrix-assisted laser desorption ionization mass spectrometer (MALDI-TOF-MS). Thermogravimetric analysis (TGA) was conducted on a Perkin-Elmer TGA-7 with a heating rate of 10 K/min under nitrogen. UV-Vis absorption spectra were recorded on the SHIMADZU UV-2600 spectrophotometer. The cyclic voltammetry results were obtained with a computer-controlled CHI 660E electrochemical workstation.

The morphologies of the PM6/acceptor blend films were investigated by atomic force microscopy (AFM, Agilent Technologies, 5500 AFM/SPM System, USA) in contacting mode with a 5 μm scanner. Transmission electron microscopy (TEM) measurements were performed in a JEM-2100F. Samples for the TEM measurements were prepared as following: The active layer films were spin-cast on ITO/ PEDOT: PSS substrates, and the substrates with active layers were submerged in deionized water to make the active layers float onto the air-water interface. Then, the floated films were picked upon unsupported 200 mesh copper grids for the TEM measurements.

Grazing Incidence Wide-Angle X-ray Scattering (GIWAXS) measurements were accomplished with a Xeuss 2.0 SAXS/WAXS laboratory beamline using a Cu X-ray source (8.05 keV, 1.54 Å) and a Pilatus3R 300K detector. The incidence angle is 0.2º. GIWAXS samples are prepared on silicon substrate by spin coating.

3. Device fabrication and characterization

The optimized solar cell devices were fabricated with a conventional structure of Glass/ITO/PEDOT: PSS (40 nm)/PM6: Acceptors/PFN-Br (5nm)/Ag. Pre-patterned ITO coated glass substrates (purchased from Advanced Election Technology Co., Ltd) were washed with deionized water and isopropyl alcohol in an ultrasonic bath for 15 minutes each. After blow-drying with high-purity nitrogen, all ITO substrates are cleaned in the ultraviolet ozone cleaning system for 25 minutes. Subsequently, a thin layer of PEDOT: PSS (Xi'an Polymer Light Technology Corp 4083) was deposited through spin-coating on pre-cleaned ITO-coated glass at 5000 rpm for 25 s and dried subsequently at 150°C for 15 minutes in atmospheric air. Then the photovoltaic layers were spin-coated in a glovebox from a solution of PM6: acceptor (14 mg/mL with 0.5 vol% 1-chloronaphthalene (CN)) with the PM6/acceptor weight ratios of 1:1.2 in CF. The optimal active layers were fabricated by spin-coating at about 3400 rpm for the 30s. Then the PM6: acceptor films were treated with thermal annealing at 110℃ for 10 min. After cooling to room temperature, a PFN-Br layer via a solution concentration of 0.5 mg/mL was deposited at the top of the active layer at a rate of 3000 rpm for 30 s. Finally, the top Ag electrode of 100 nm thickness was thermally evaporated through a mask onto the cathode buffer layer under a vacuum of 1.5×10^{-4}mbar. Current density–voltage (*J*–*V*) curves of the devices were performed by a Keithley 2400 source meter in a glove box with a nitrogen atmosphere. The simulated sunlight was calibrated by an AM 1.5G solar simulator (Enlitech, SS-F5, Taiwan), which was measured with a calibrated Si diode from National Renewable Energy Laboratory. The EQE curves were tested by an EnLi Technology (Taiwan) EQE measurement system.

Electron mobility and hole mobility measurements. The electron mobility device adopted the ITO/ZnO/active layer/PDINN/Al structure, and the hole mobility device adopted the ITO/PEDOT: PSS/Active layer/MoO_3/Ag structure. The electron and hole mobilities were calculated according to the space charge limited current (SCLC) method by the equation: $J = 9\mu\varepsilon_r\varepsilon_0 V^2/8d^3$, where J is the current density, μ is the electron or hole mobility, V is the internal voltage in the device, ε_r is the relative dielectric constant of active layer material, ε_0 is the permittivity of empty space, and d is the thickness of the active layer.

4. ^{1}H NMR, ^{13}C NMR, and High-Resolution Mass (MOLDI-TOF) Spectra

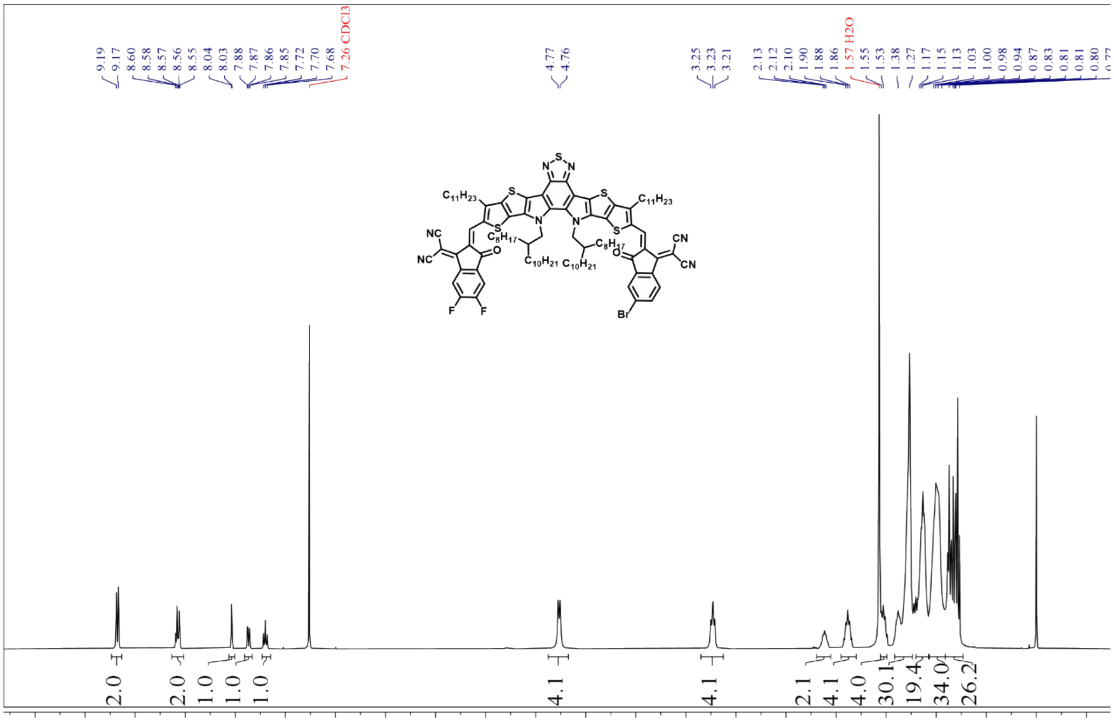

Figure S5. ^{1}H NMR spectrum of BTP-2F-Br in $CDCl_3$.

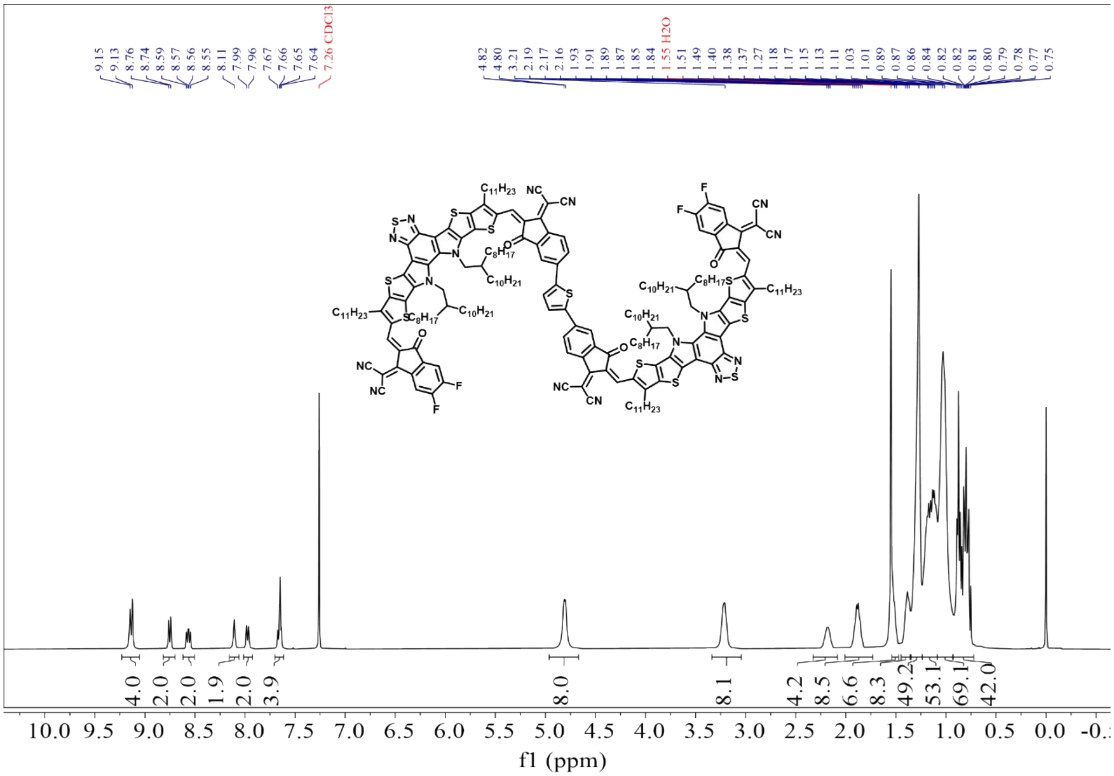

Figure S6. ^{1}H NMR spectrum of **QM-1T** in CDCl$_3$.

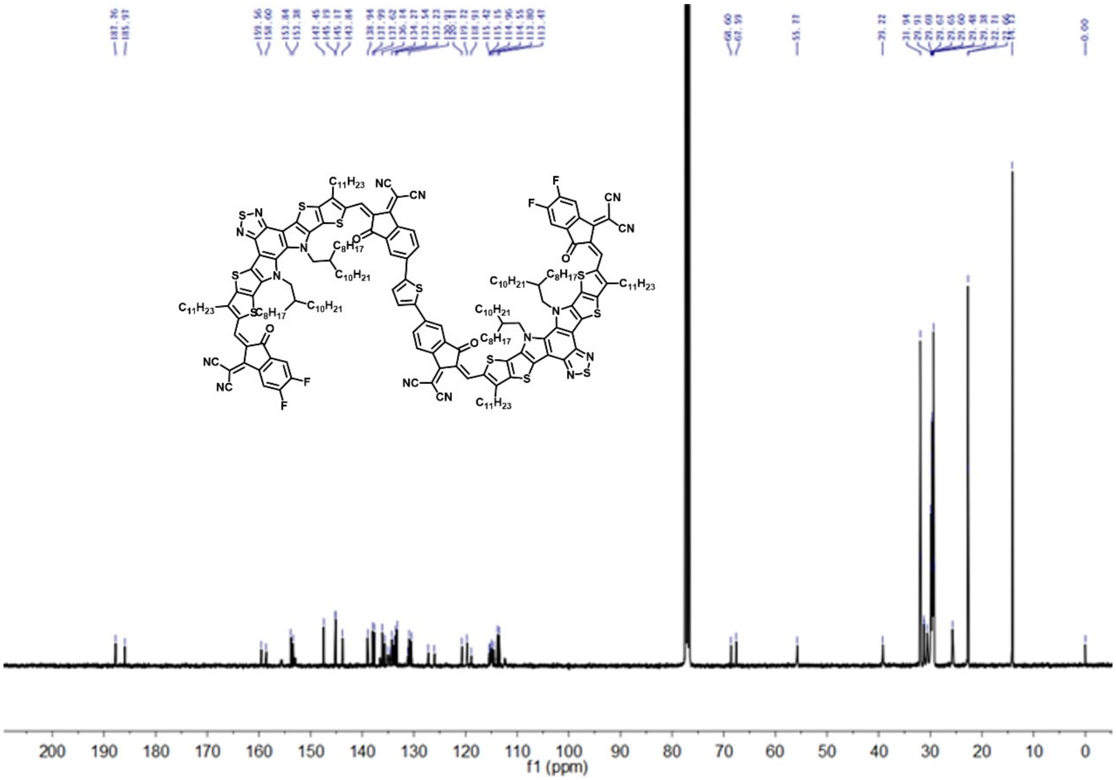

Figure S7. ^{13}C NMR spectrum of **QM-1T** in CDCl$_3$.

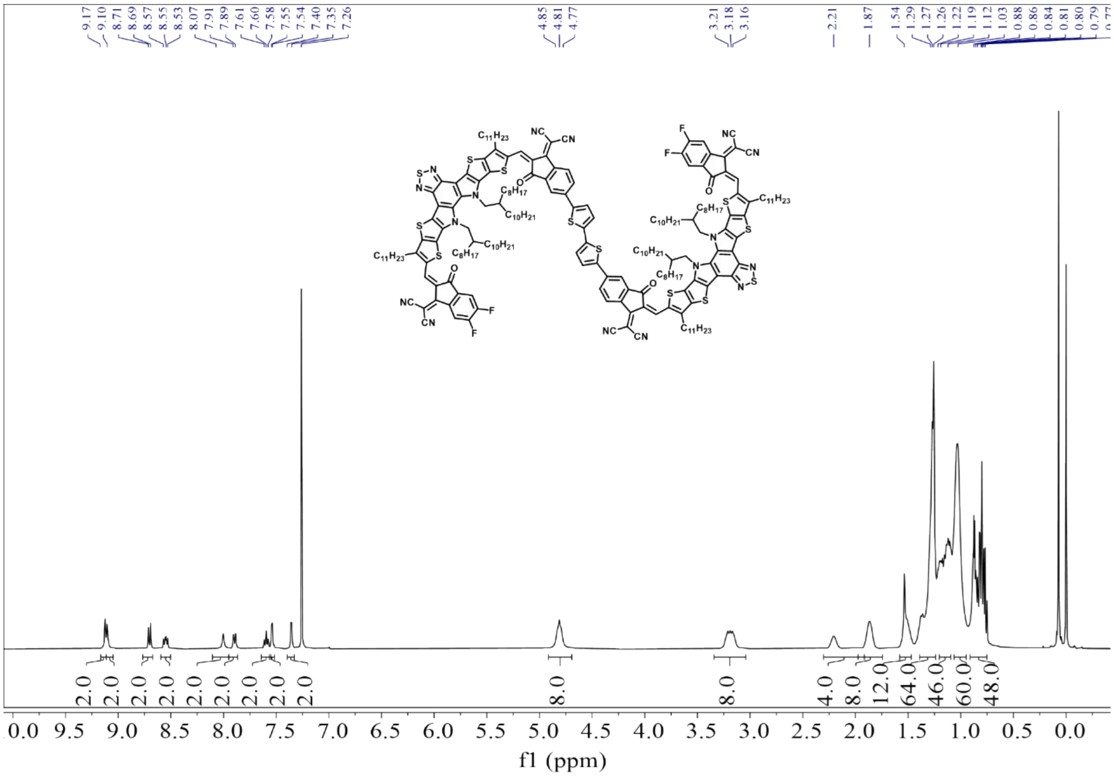

Figure S8. ^{1}H NMR spectrum of **QM-2T** in $CDCl_3$.

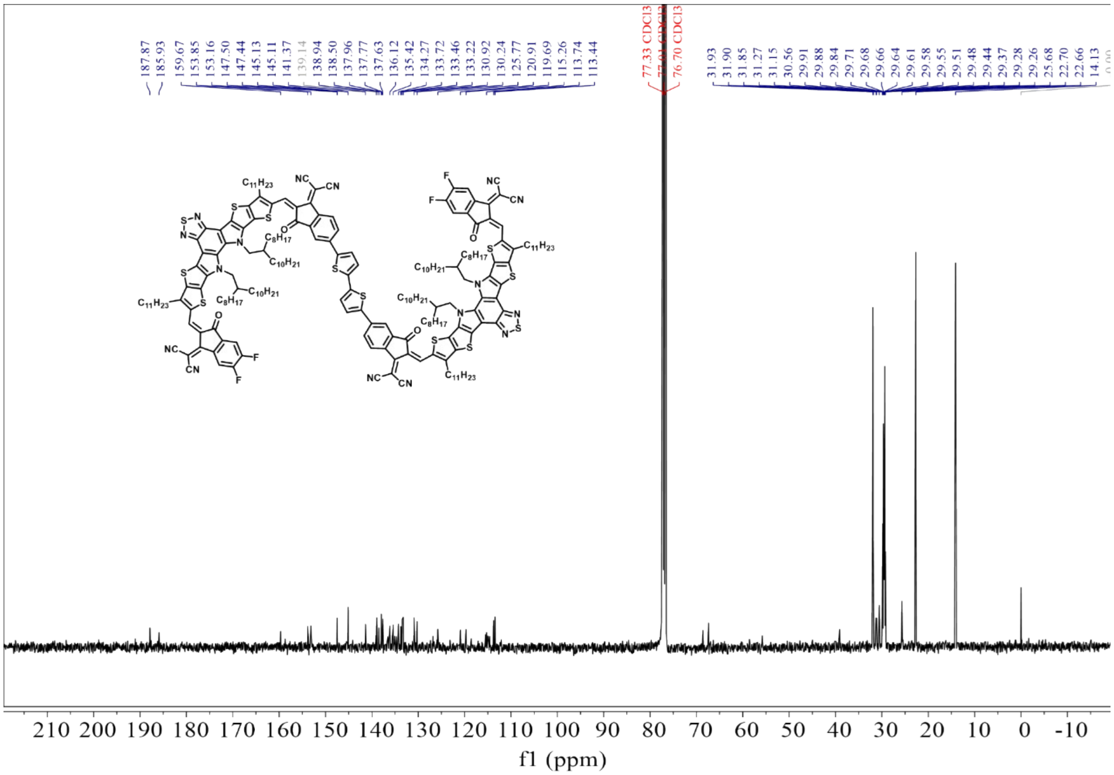

Figure S9. ^{13}C NMR spectrum of **QM-2T** in $CDCl_3$.

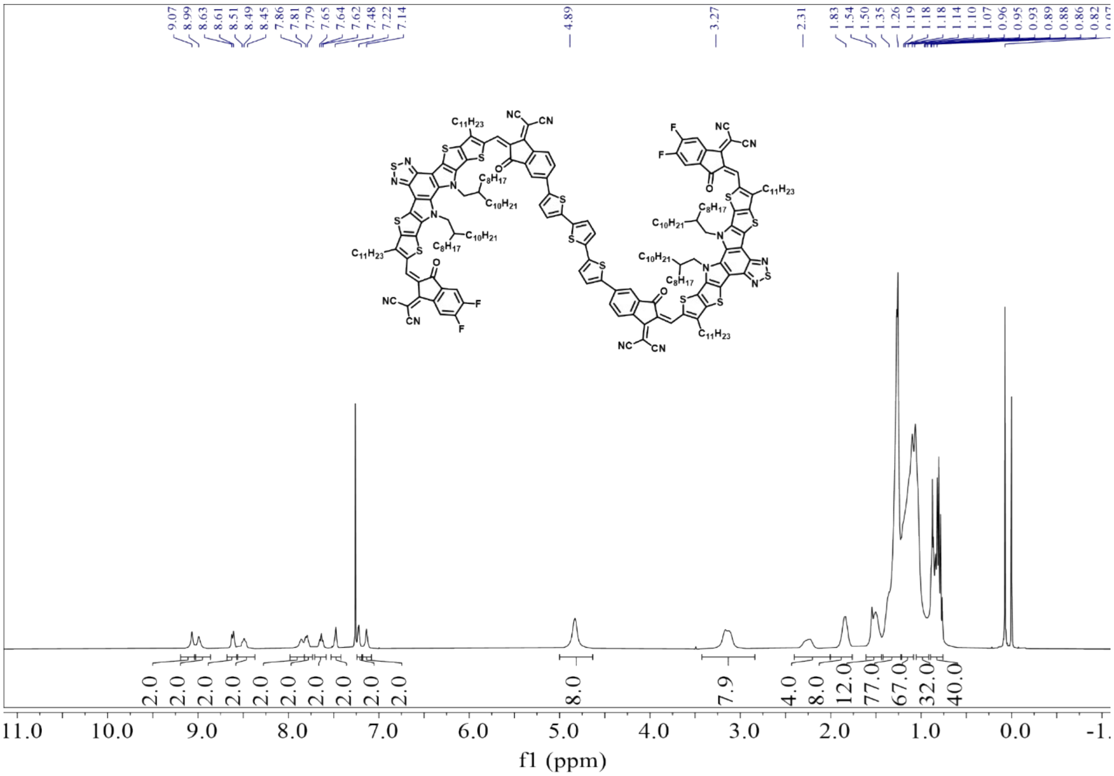

Figure S10. ^{1}H NMR spectrum of **QM-3T** in $CDCl_3$.

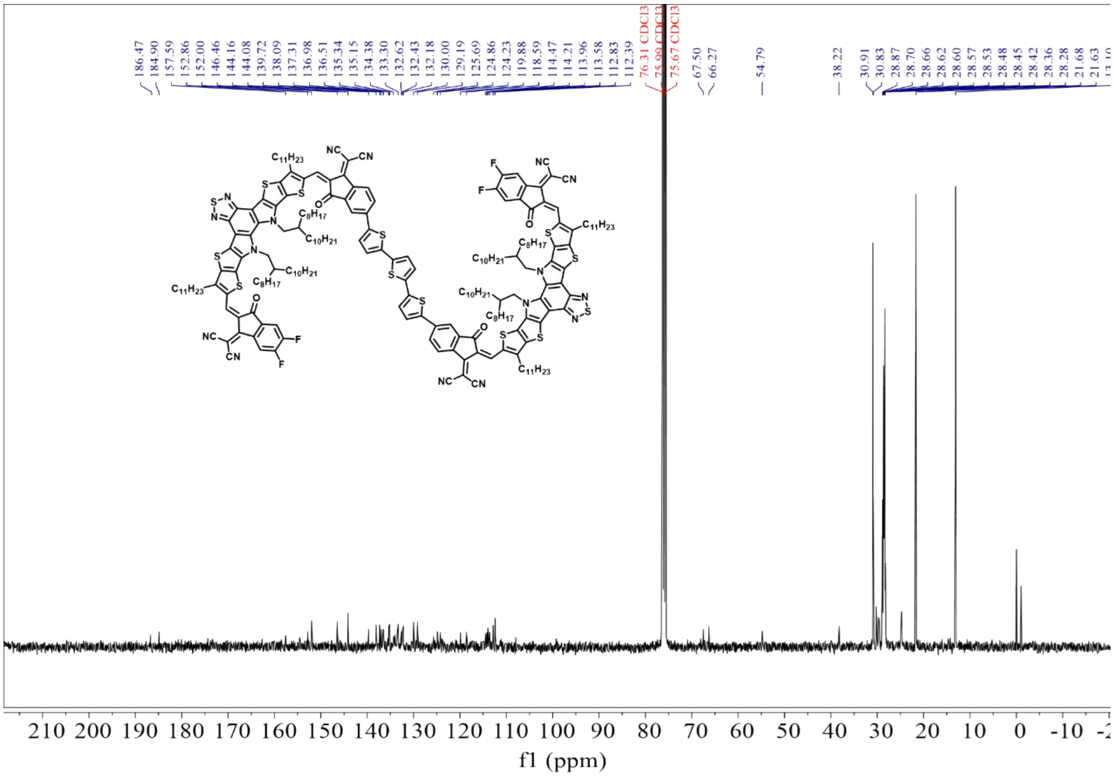

Figure S11. ^{13}C NMR spectrum of **QM-3T** in $CDCl_3$.

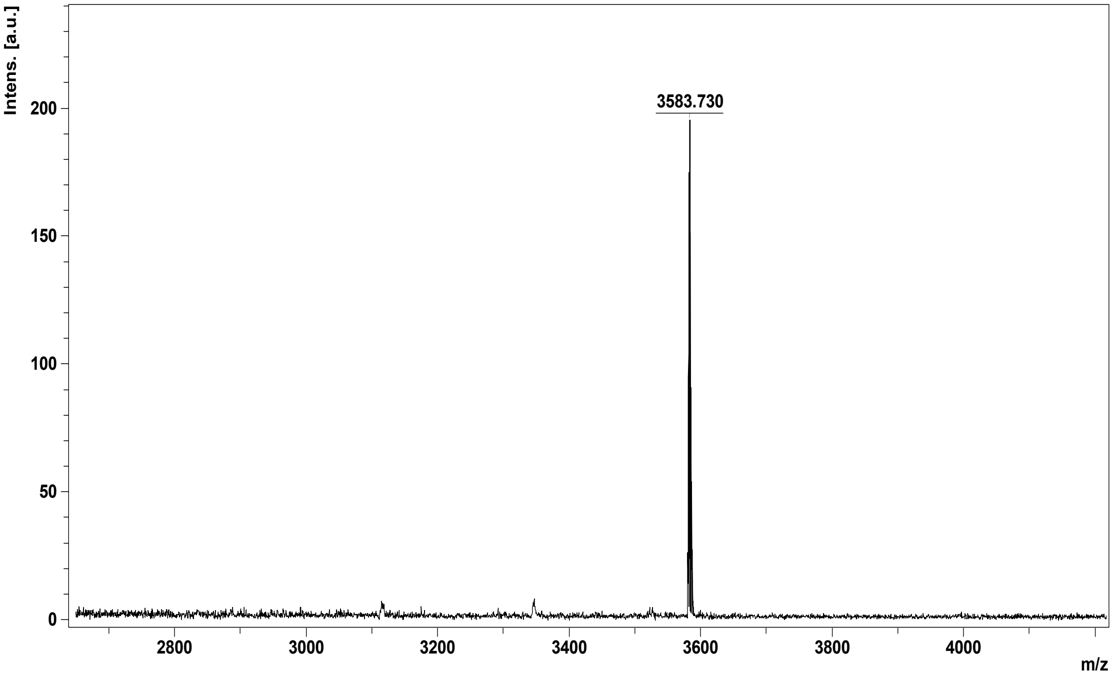

Figure S12. The high-resolution mass spectrum (MALDI-TOF) of **QM-1T** in $CDCl_3$.

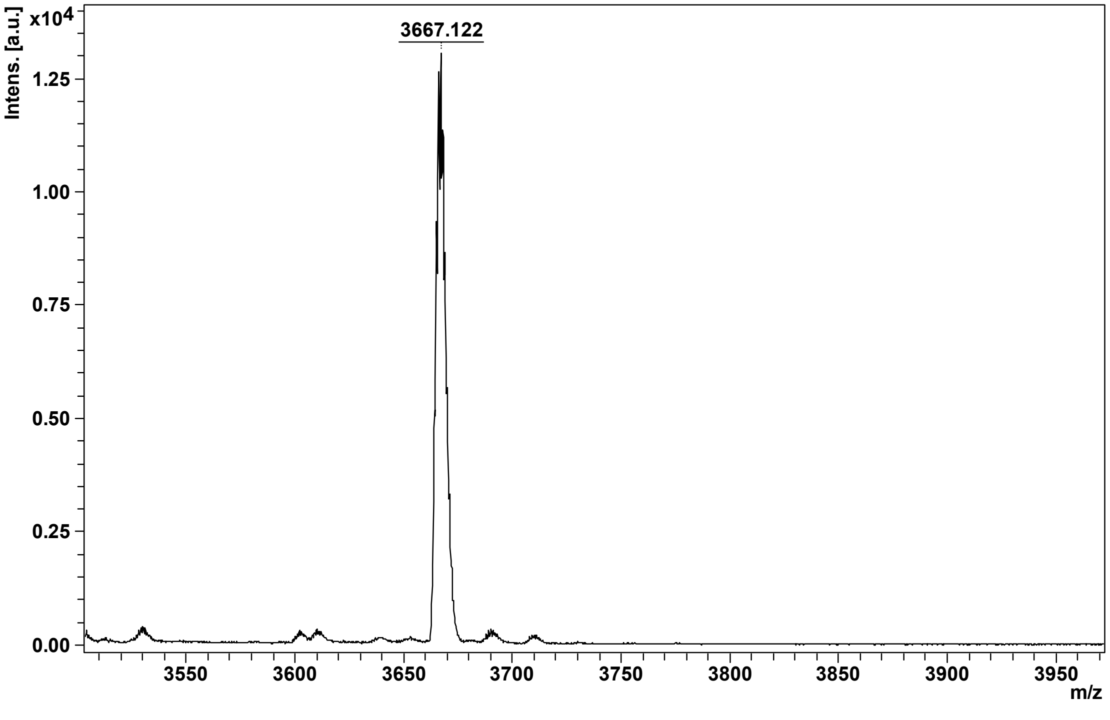

Figure S13. The high-resolution mass spectrum (MALDI-TOF) of **QM-2T** in $CDCl_3$.

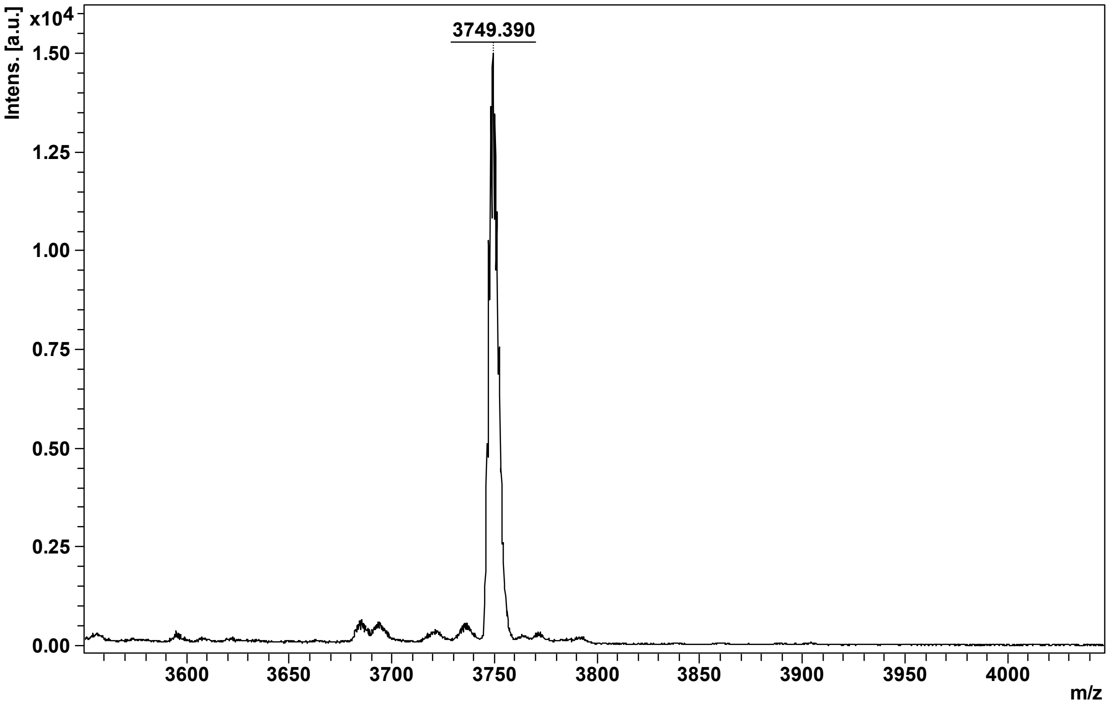

Figure S14. The high-resolution mass spectrum (MALDI-TOF) of **QM-3T** in $CDCl_3$.

5. Additional Figures and Tables

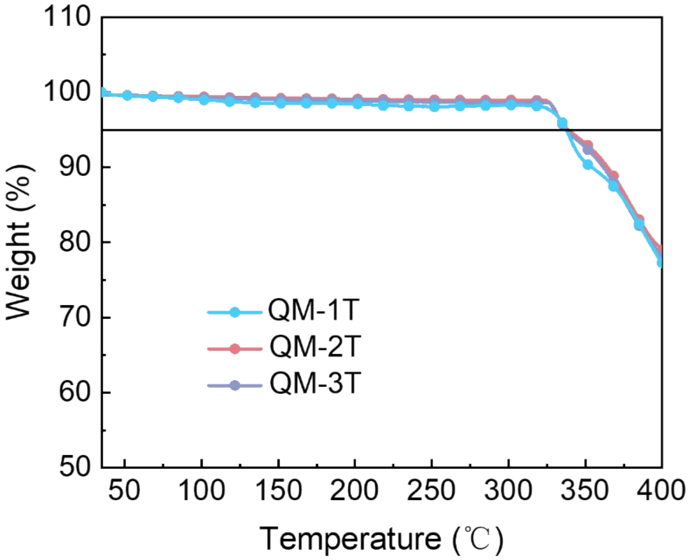

Figure S15. Thermogravimetric analysis curves of **QM-2T** and **QM-3T** with a heating rate of 10 °C·min^{-1}.

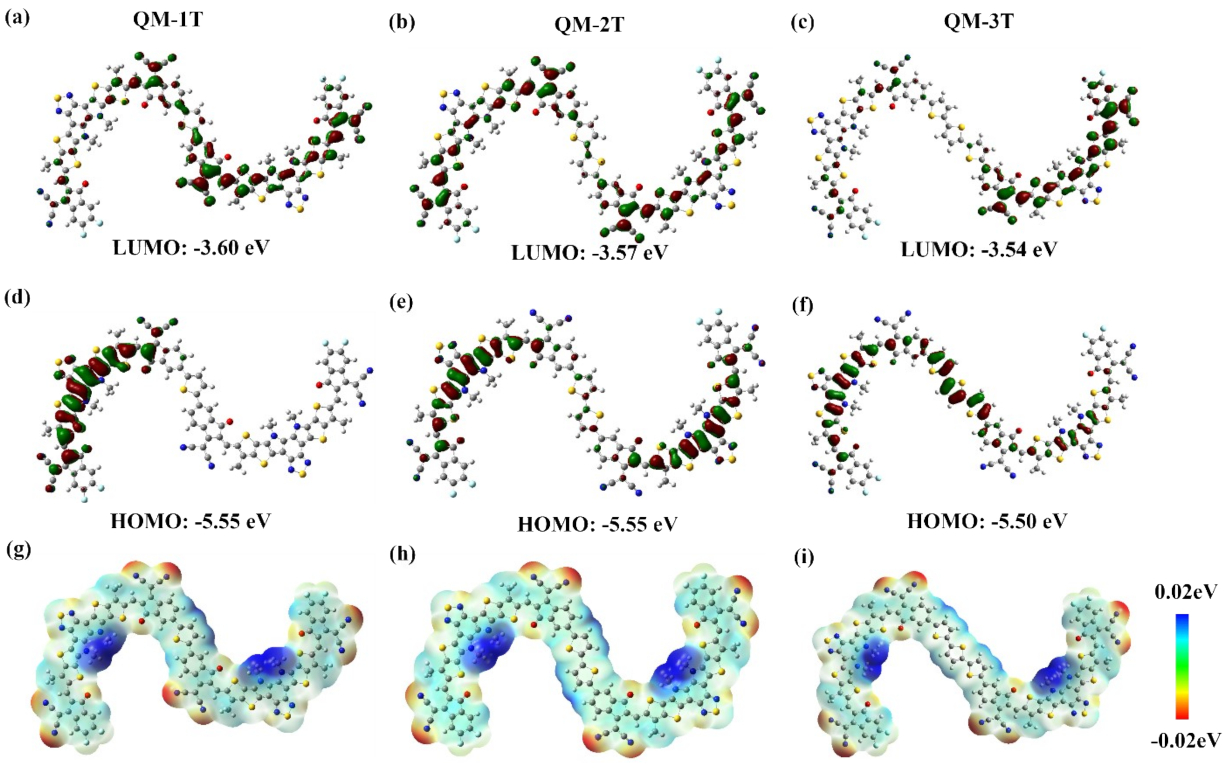

Figure S16. (a-f) DFT calculated LUMO/HOMO and the corresponding energy levels of QM-1T, QM-2T and QM-3T, respectively; (g-i) Electrostatic potential surfaces of QM-1T, QM-2T and QM-3T molecules.

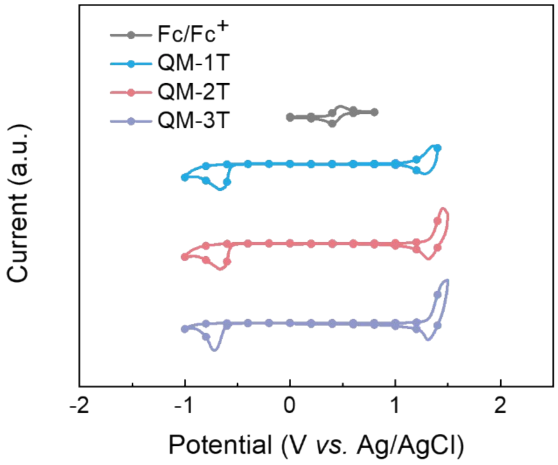

Figure S17. Cyclic voltammogram of QM1, QM-2T and QM-3T in acetonitrile solution with 0.1 M Bu_4PF_6 as the supporting electrolyte, at with a scanning rate of 50 mV s^{-1}.

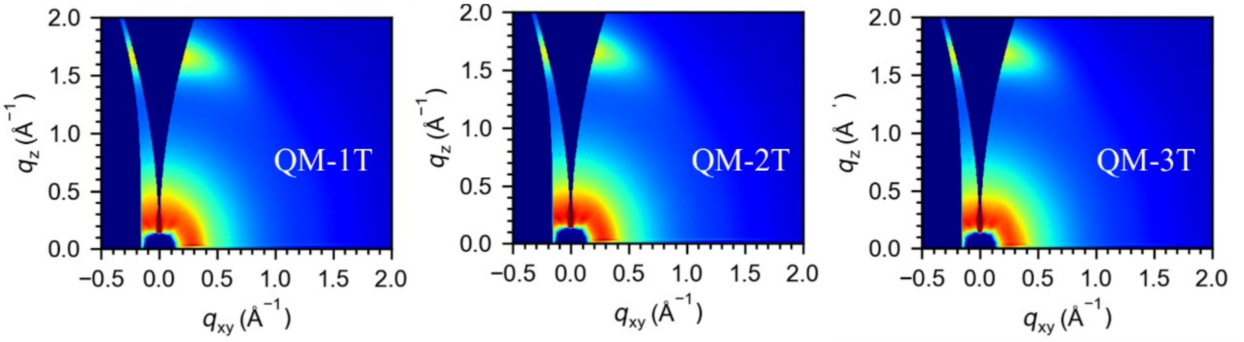

Figure S18. 2D-GIWAXS diffraction patterns of (a) **QM-1T**, (b) **QM-2T** and (c) **QM-3T** films processed with CF.

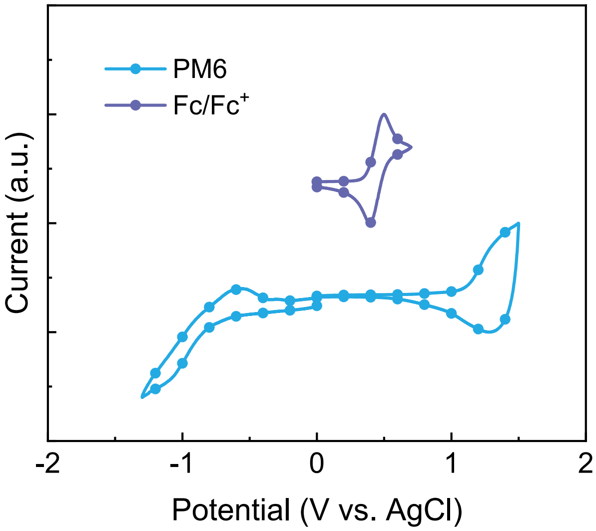

Figure S19. Cyclic voltammogram of PM6 in acetonitrile solution with 0.1 M Bu_4PF_6 as the supporting electrolyte, at with a scanning rate of 50 mV s^{-1}.

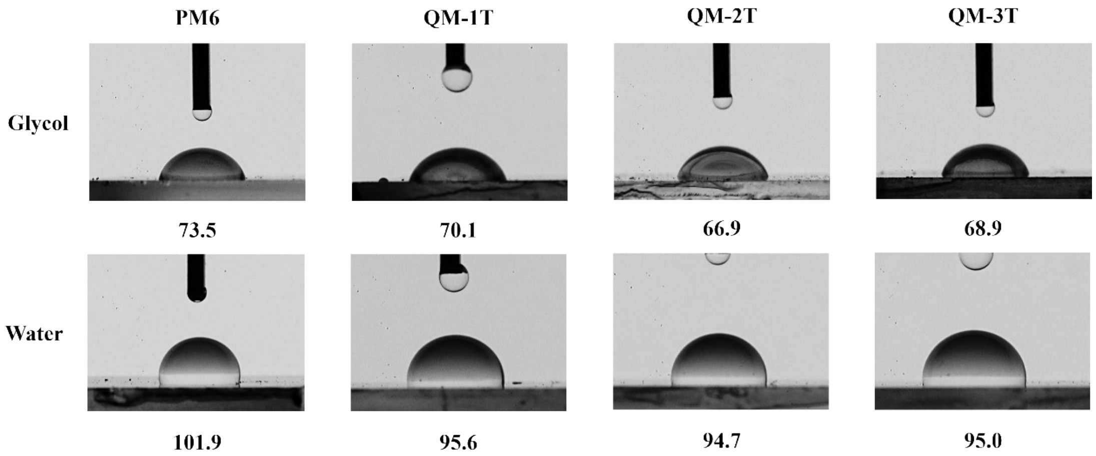

Fig S20. Contact angle images of water and ethylene glycol droplets on the neat films of PM6, QM-1T, QM-2T and QM-3T.

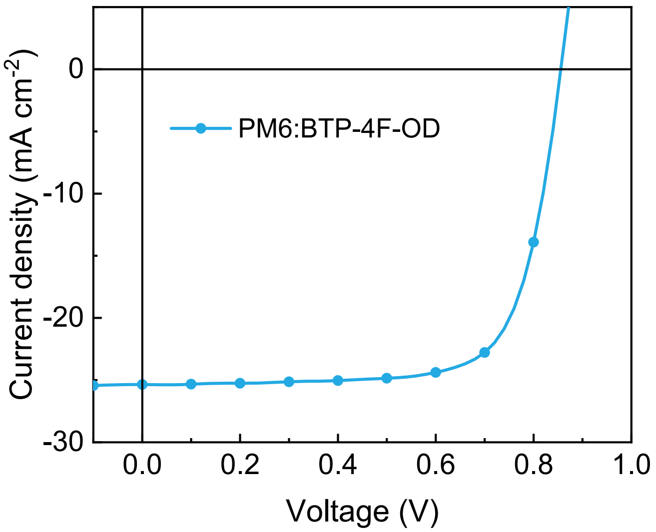

Fig. S21. $J-V$ curves of the corresponding device.

Table S1. Optimal photovoltaic parameters of the OSC based on BTP-4F-OD under 1 sun illumination

Active layer	V_{OC} (V)	J_{SC} (mA/ cm^2)	FF (%)	PCE (%)
PM6:BTP-4F-OD	0.855	25.35	73.51	15.94

Table S2. Statistics of V_{OC} and corresponding J_{SC} values for binary OSCs based on PM6 and **A-π-A** type QM acceptors.

Acceptors	V_{OC} (V)	J_{SC} (mA/ cm^2)	FF (%)	PCE (%)	Reference
CHD1	0.949	23.90	73	16.62	2
CH8-0	0.936	22.61	72	15.26	3
CH8-1	0.923	24.89	74	17.05	3
CH8-2	0.928	24.24	75	16.84	3
dBTIC-δV-BO	0.960	20.67	66	13.15	4
dBTIC-γV-BO	0.910	24.52	77	17.14	4
dBTIC-γV-OD-2Cl	0.870	24.65	74	16.04	4
EV-i	0.897	26.60	76	18.27	5
QM2	0.910	25.42	71	16.36	1
DIBP3F-Se	0.917	25.92	76	18.09	6
DIBP3F-S	0.901	24.86	72	16.11	6
Dimer-QX	0.933	22.57	69	14.59	7
Dimer-2CF	0.889	25.27	80	18.12	7
2BTP-2F-T	0.925	24.35	73	16.54	8
DYV	0.910	25.97	76	18.01	9
DYVC	0.915	24.87	74	16.81	9
DYTVT	0.935	22.90	68	14.59	9
DYB	0.939	20.51	67	12.98	9
DYT	0.940	24.08	76	17.30	10
DYV	0.930	25.64	78	18.60	10
DYTVT	0.950	24.82	74	17.68	10
DYSe-I	0.940	23.50	74	16.80	11
DYSe-O	0.950	19.70	69	14.00	11
DYBO	0.968	24.62	75	18.08	12

Table S3. Contact angle and statistical data of surface tension and interaction parameter.

Materials	Water	Glycol	γd (mN m^{-1})	γp (mN m^{-1})	γ (mN m^{-1})	χ/ $K(\gamma D^{-2}-\gamma A^{-2})^2$
PM6	101.9	73.5	27.18	0.71	27.89	/
QM-1T	95.6	70.1	22.46	2.74	25.21	0.068
QM-2T	94.7	66.9	26.09	2.30	28.38	0.002
QM-3T	95.0	68.9	23.38	2.73	26.11	0.029

References:

1. W. Liu, J. Yuan, C. Zhu, Q. Wei, S. Liang, H. Zhang, G. Zheng, Y. Hu, L. Meng, F. Gao, Y. Li and Y. Zou, *Sci. China: Chem.*, 2022, **65**, 1374-1382.
2. Z. Li, Z. Zhang, H. Chen, Y. Zhang, Y. Q. Q. Yi, Z. Liang, B. Zhao, M. Li, C. Li, Z. Yao, X. Wan, B. Kan and Y. Chen, *Adv. Energy Mater.*, 2023, **13**, 2300301.
3. H. Chen, Z. Zhang, P. Wang, Y. Zhang, K. Ma, Y. Lin, T. Duan, T.-F. He, Z. Ma, G. Long, C. Li, B. Kan, Z. Yao, X. Wan and Y. Chen, *Energy Environ. Sci.*, 2023, **16**, 1773-1782.
4. P. Tan, H. Chen, H. Wang, X. Lai, Y. Zhu, X. Shen, M. Pu, H. Lai, S. Zhang, W. Ma and F. He, *Adv. Funct. Mater.*, 2023, **34**, 2305608.
5. H. Zhuo, X. Li, J. Zhang, S. Qin, J. Guo, R. Zhou, X. Jiang, X. Wu, Z. Chen, J. Li, L. Meng and Y. Li, *Angew. Chem., Int. Ed.*, 2023, **62**, e202303551.
6. J. Wu, Z. Ling, L. R. Franco, S. Y. Jeong, Z. Genene, J. M. Gomez, S. Chen, C. Chen, C. M. Araujo, C. F. N. Marchiori, J. Kimpel, X. Chang, F. H. Isikgor, Q. Chen, H. Faber, Y. Han, F. Laquai, M. Zhang, H. Y. Woo, D. Yu, T. D. Anthopoulos and E. Wang, *Angew. Chem., Int. Ed.*, 2023, DOI: 10.1002/anie.202302888, e202302888.
7. M. Lv, Q. Wang, J. Zhang, Y. Wang, Z. G. Zhang, T. Wang, H. Zhang, K. Lu, Z. Wei and D. Deng, *Adv. Mater.*, 2023, **36**, e2310046.
8. L. Zhang, Z. Zhang, D. Deng, H. Zhou, J. Zhang and Z. Wei, *Adv. Sci.*, 2022, **9**, e2202513.
9. H. Fu, M. Zhang, Y. Zhang, Q. Wang, Z. Xu, Q. Zhou, Z. Li, Y. Bai, Y. Li and Z. G. Zhang, *Angew. Chem., Int. Ed.*, 2023, **62**, e202306303.

10. J.-W. Lee, C. Sun, C. Lee, Z. Tan, T. N.-L. Phan, H. Jeon, D. Jeong, S.-K. Kwon, Y.-H. Kim and B. J. Kim, *ACS Energy Lett.*, 2023, **8**, 1344-1353.
11. H. Jeon, K.-p. Hong, J.-W. Lee, D. Jeong, T. N.-L. Phan, H.-G. Lee, J. S. Park, C. Wang, S. Xuyao, Y.-H. Kim and B. J. Kim, *Chem. Mater.*, 2023, **35**, 9276-9286.
12. C. Sun, J.-W. Lee, C. Lee, D. Lee, S. Cho, S.-K. Kwon, B. J. Kim and Y.-H. Kim, *Joule*, 2023, **7**, 416-430.